Grapefruit-derived Nanovectors Delivering Therapeutic miR17 Through an Intranasal Route Inhibit Brain Tumor Progression

Xiaoying Zhuang[1], Yun Teng[1], Abhilash Samykutty[1], Jingyao Mu[1], Zhongbin Deng[1], Lifeng Zhang[1], Pengxiao Cao[1], Yuan Rong[1], Jun Yan[1], Donald Miller[1] and Huang-Ge Zhang[1,2]

[1]Brown Cancer Center, Department of Microbiology and Immunology, University of Louisville, Louisville, Kentucky, USA; [2]Robley Rex Veterans Administration Medical Center, Louisville, Kentucky, USA

The lack of access to the brain is a major obstacle for central nervous system drug development. In this study, we demonstrate the capability of a grapefruit-derived nanovector (GNV) to carry miR17 for therapeutic treatment of mouse brain tumor. We show that GNVs coated with folic acid (FA-GNVs) are enhanced for targeting the GNVs to a folate receptor-positive GL-26 brain tumor. Additionally, FA-GNV-coated polyethylenimine (FA-pGNVs) not only enhance the capacity to carry RNA, but the toxicity of the polyethylenimine is eliminated by the GNVs. Intranasal administration of miR17 carried by FA-pGNVs led to rapid delivery of miR17 to the brain that was selectively taken up by GL-26 tumor cells. Mice treated intranasally with FA-pGNV/miR17 had delayed brain tumor growth. Our results demonstrate that this strategy may provide a noninvasive therapeutic approach for treating brain-related disease through intranasal delivery.

Received 29 May 2015; accepted 22 September 2015; advance online publication 3 November 2015. doi:10.1038/mt.2015.188

INTRODUCTION

A large number of drugs with therapeutic potential for treatment of brain-related diseases are never pursued due to their inability to be delivered across the blood–brain barrier in therapeutic concentrations. Although intranasal delivery provides a practical, noninvasive method for delivering therapeutic agents to the brain, the quantities of drug administered nasally that have been shown to be transported directly from nose to brain are very low.[1–3] Although our results suggest that intranasal delivery of an anti-inflammatory agent such as curcumin, and the anti-Stat3 agent, JSI-124, provides a promising noninvasive approach for the treatment of brain inflammatory-related diseases such as malignant gliomas,[4] biosafety considerations and large-scale production of mammalian cell-derived exosomes has been challenging. To meet this challenge, we recently developed fruit-based nanovectors made of lipids extracted from edible plant exosomes. Exosome-like nanoparticles from grapefruit naturally encapsulate small RNAs and proteins. We have shown that grapefruit-derived nanovectors (GNVs) are highly efficient for delivering a variety of therapeutic agents including drugs, DNA expression vectors, siRNA, and antibody in mouse model studies without inducing toxicity.[5,6]

Using GNVs for intranasal delivery of therapeutic agents has not been addressed. In this study, we developed a GNV-based nanovector hybrid with polyethylenimine (PEI) (pGNV) for effective intranasal delivery of miRNA to brain. The reason for using PEI as an enhancer for delivering nucleic acid is that PEI has a higher efficiency in carrying RNA and DNA. However, PEI is toxic due to the positive charge on the surface of the PEI particles.[7,8] Positively charged PEI polyplexes are required for high-efficient transfection; in the absence of the free net positive charge PEI polyplexes, intracellular elimination of nucleic acids is faster. The toxicity of the PEI is reduced by making hybrid the PEI polyplexes with GNVs. Enhanced targeting was further achieved by coating pGNVs with the tumor targeting moiety, FA. This allowed for active targeting of cancer cells to potentiate the transfection efficiencies of brain cancer cells *in vitro* and *in vivo*. This study therefore provides an effective approach to overcome the efficiency–toxicity challenges faced with nonviral vectors. This study provides insights into the design strategy of effective and safe vectors for cancer gene therapy.

RESULTS

Intranasally administered GNVs are transported to the brains of mice

Using standard techniques,[6] we isolated edible plant exosome-like nanoparticles from the juice of grapefruit, and nanoparticles were made with lipids extracted from grapefruit exosome-like nanoparticles. The nanoparticles were fully characterized based on electron microscopic examination (**Supplementary Figure S1a**) of a sucrose gradient purified band, charge, and size distribution (**Supplementary Figure S1b**).

To determine whether GNVs can be transported intranasally into the brain, DIR-dye-labeled GNVs were administered using a small pipette as ten 2-µl doses in alternating sides of the nose spaced 2 minutes apart. Twelve hours after intranasal delivery, mouse brains were examined for the presence of the GNVs using an Odyssey scanner. DIR fluorescent-labeled GNVs were observed in the brain with their primary location being in the olfactory bulb, hippocampus, thalamus, and cerebellum, suggesting that translocation of GNVs to the brain occurred within a short time (**Figure 1**). In contrast, a standard liposome, DOTAP, commonly used for gene transfer, was not detected in the brain (**Figure 1**).

Correspondence: Huang-Ge Zhang, James Brown Cancer Center, Department of Microbiology and Immunology, University of Louisville, CTRB 309, 505 Hancock Street, Louisville, Kentucky 40202, USA. E-mail: H0Zhan17@louisvile.edu

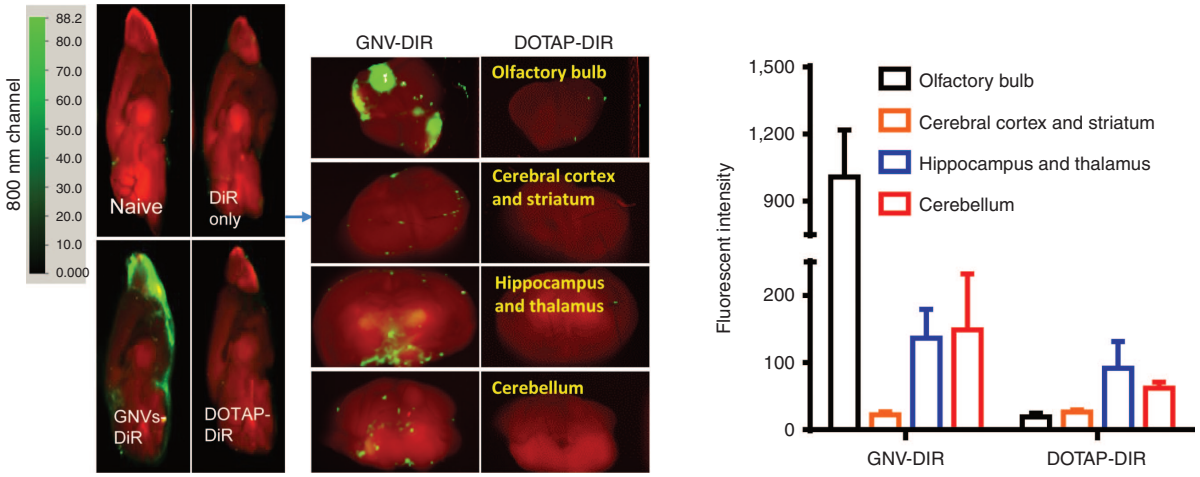

Figure 1 Intranasal administration of GNVs results in localization to the brain. DIR-labeled GNVs (green) or controls were administered intranasally into C57BL/6j mice. (**a**) 12 hours of postintranasal administration, the brain was cut sagittally or coronally for imaging using the Odyssey laser-scanning imager. Representative images from the center of the brain ($n = 5$) are shown. Results were obtained from three independent experiments with five mice in each group of mice.

Very little or no fluorescence was detected in the brain of mice intranasally administered phosphate-buffered saline (PBS) or free DIR-dye (Figure 1). These results suggest that GNVs have a unique property allowing for intranasal transfer or delivery to the brain. No apparent toxicity or behavioral abnormalities such as diarrhea, altered gait or skin inflammation, swelling, ulceration of the body or motor paralysis were observed in any of the mice during and after (21 days) the experiment.

RNA carried by GNVs is intranasally delivered to brain

Given that intranasally administered GNVs are transported to the brains of mice and that delivering RNA through an intranasal route would have numerous applications for gene therapy of brain-related diseases, we next tested whether RNA carried by GNVs can be delivered without degradation to the brain. First, we tested whether the efficiency of GNVs for delivering RNA in general can be increased using PEI due to the reported higher efficiency of PEI in carrying RNA and DNA.[7] Increasing the capacity of RNA or DNA being encapsulated for potential intranasal delivery is an important factor because one of the limiting factors in the intranasal delivery is the amount of therapeutic reagents successfully delivered. To test this concept, total RNAs were extracted from EL4 cells. PEI and cellular RNA were mixed (PEI/RNA) and subsequently added to lipid film extracted from grapefruit exosome-like nanoparticles and followed by sonication. The results showed that the PEI/RNA reassembled into GNVs (pGNV/RNA) with a diameter of 87.2 ± 11.3 nm (means ± SEM), whereas PEI/RNA has a diameter of 35.6 ± 8.7 nm (Figure 2a). Data presented in Figure 2a (top panel) are supported by (i) Electron microscopy examination showing that the PEI/RNA complex is smaller than the pGNV/RNA in size (Figure 2a, bottom panel); (ii) the location of pGNV/RNA after sucrose gradient centrifugation where it migrated to a different density than that of GNV/RNA which do not have PEI (**Supplementary Figure S2**); and (iii) pGNV/RNA has a higher sucrose density than GNVs (1.11 versus 1.03; **Supplementary Figure S2**). Zeta potential values for the PEI/RNA complex were positive, whereas pGNVs were negative. Values were in the range of 20.9 mV for the PEI/RNA complex and −13.9 mV for the pGNV/RNA complexes (Figure 2b). Remarkably, the results generated from quantitative analysis of RNA extracted from pGNV/RNA and GNV/RNA indicate that the capacity of pGNVs to carry RNA is much higher (86.2 ± 5.7%) than the GNVs (5.9 ± 1.6%; Figure 2c). Next, we tested whether the RNA carried by pGNVs can be delivered to the brain through an intranasal route. Total RNAs extracted from the EL4 cell line were labeled with the fluorescent dye Syto60 for tracking RNA delivered by pGNVs. The imaging results from frozen sectioned brain indicated that a positive fluorescent signal was detected as early as 1.5 hours after intranasal administration (Figure 2d). The Syto60-labeled RNA signal was detected primarily in the olfactory bulb, midbrain, and thalamus 12 hours after intranasal administration. The size and charge of nanoparticles has an effect on their distribution *in vivo*. The fact that pGNVs are smaller in size than GNVs (**Supplementary Figure S1**) prompted us to further determine whether physiological distribution of pGNVs is different from that of GNVs after intranasal administration. The imaging results from frozen sectioned brain indicated that a stronger fluorescent signal was detected in the thalamus and midbrain of mice given pGNV/RNA than of mice given GNV/RNA. This result agrees with a reduction of DiR signal 12 hours postadministration that is detected in the olfactory bulb of mice given pGNV/RNA (Figure 2e).

PEI and nucleic acid complexes are toxic and directly linked to the positive charge on the surface of the complex.[7,9] Next, we tested whether PEI/RNA complexed with GNVs is less toxic than PEI/RNA. Immune histological staining indicates that intranasal administration of PEI/RNA induces a large number of F4/80$^+$ macrophages and Iba-1$^+$ microglia cells, whereas no induction was observed in the brain of mice intranasally administrated with pGNV/RNA in comparison with mice given PBS as a control (Figure 2f). A lack of induction of F4/80$^+$ macrophages and Iba-1$^+$ microglia cells is most likely not due to a reduced amount of PEI in PEI/RNA when compared to pGNV/RNA since there was approximately the same amount of PEI detected in the PEI/RNA

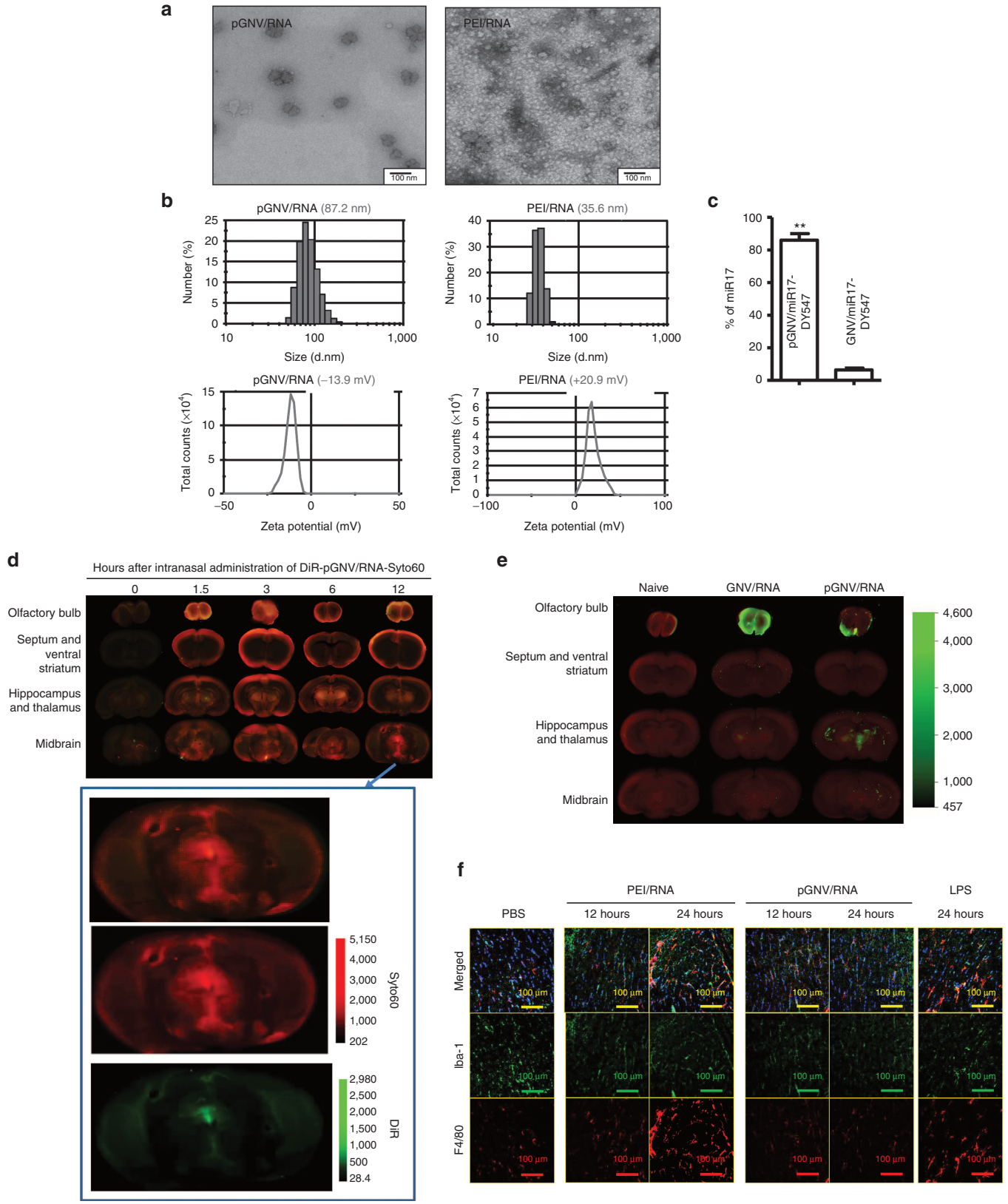

Figure 2 pGNVs have a better capacity for carrying RNA without toxicity. RNA loaded pGNVs (pGNV/RNA) and PEI-RNA were purified by ultracentrifugation. (**a**) Sucrose-banded pGNV/RNA and PEI-RNA were visualized and imaged by electron microscopy. (**b**) Size distribution (top panel) and Zeta potential (bottom panel) of pGNV/RNA) or PEI/RNA were analyzed using a ZetaSizer. (**c**) Loading efficiency of miR17-Dy547 was determined using a fluorescence microplate reader (EX/Em = 530/590 nm) and expressed as % = (miR17-DY547 in pGNV/RNA or GNVs)/total RNA used for loading × 100%. Images (**a, b**) and data (**c**, $n = 5$) are representative of at least three independent experiments. (**d**) Intranasal administration of pGNV/RNA-Syto60 results in localization to the brain. Syto60-labeled RNA (20 μg, red) carried by DIR-labeled pGNVs (green) was administered intranasally

and pGNV/RNA (**Supplementary Figure S3**). Collectively, combination of PEI and GNVs enhances the delivering RNA efficiency in GNVs and eliminates the toxicity induced by PEI vector.

Intranasal targeted delivery of miR17 to brain tumor with FA-pGNVs

Since no adverse side effects have been observed with an intranasal administration of pGNVs, we next tested whether pGNVs can be used as a therapeutic miRNA delivery vehicle. In cancer therapy, accurate targeting to tumor tissue is required for successful therapy. Therefore, we first tested whether pGNVs can be modified to achieve tumor targeting. High-affinity folate receptors (FRs) are expressed at elevated levels on many human tumors and in almost negligible amounts on nontumor cells.[10–16] Therefore, we tested whether pGNVs binding folic acid (FA) (FA-pGNVs) would significantly enhance pGNV targeting to GL-26 tumor cells which express FRs (**Supplementary Figure S4**).

To evaluate the potential use of FA-pGNVs as a targeting vector to deliver therapeutic agents to brain tumor, the efficient uptake of FA-pGNVs by GL-26 brain tumor cells was first evaluated in *in vitro* cell culture. GL-26-luc cells were co-cultured with FA-pGNVs or pGNVs carrying Dylight547 fluorescent dye-labeled RNA. The presence of FA-pGNV/RNA and pGNV/RNA in GL-26-luc cells was examined using confocal microscopy (**Figure 3a**, top panel) and determined by quantitative analysis of the numbers of Dylight547-labeled RNA$^+$ cells. The results indicated that the majority of GL26 cells internalized the FA-pGNV/RNA. More than 80% of the GL-26 cells took up the FA-pGNV/RNA within 2 hours of co-culture in comparison with 20% of the GL-26 cells taking up pGNVs/RNA. The fact that FA-coated GNVs have better transfection efficiency was also demonstrated in GL-26 cells transfected with Syto60-labeled RNA/PEI complexed with GNVs (FA-GNV/RNA-syto60) (**Figure 3a**, bottom panel). The amount of RNAs accumulating in the cells continuously increased and reached a plateau at 6 hours after transfection (**Figure 3b**). Pre-mixing FA-pGNV/RNA with the free form of FA led to a reduction of RNAs accumulating in the GL-26 cells in a FA dose-dependent manner (**Figure 3c**). This suggests that the enhanced internalization of FA-pGNV/RNA is FA receptor mediated.

We next sought to determine whether FA-pGNV/RNA has an enhanced efficiency in targeting brain tumor cells in a mouse model. Biodistribution of DiR-labeled FA-pGNV/RNA was evaluated in mice using the Odyssey imaging system. For these studies, groups of mice bearing intracerebral tumors (**Figure 3d**, top panel, and bottom panel, the first column from the right) were intranasally administrated DIR dye-labeled FA-pGNV/miR17-DY547 or pGNV/miR17-DY547. The amount of DIR$^+$ FA-pGNV/miR17-DY547 or pGNV/miR17-DY547 present after administration was quantitatively analyzed. Imaging data showed a statistically significant increase in brain tumor (**Figure 3d**, middle panel) associated photons in FA-pGNV/miR17-DY547-treated mice when compared to pGNV/miR17-DY547. This result is further supported by increased fluorescent DY547-labeled RNA signals detected in the brain tumor (**Figure 3d**, bottom panel, second columns from right) and co-localized with GL-26 cells that have high density of FRs expressed (**Figure 3d**, bottom panel, first column from left).

Intranasal targeted delivery of miR17 encapsulated in FA-pGNVs inhibits GL26 tumor growth

Finally, we determined whether miR17 carried by FA-pGNVs has a therapeutic effect in a mouse brain tumor model. We begin with testing whether RNA carried by the FA-pGNVs still has biological activity. To address this issue, we used a well-characterized siRNA that is directed against a luciferase reporter gene stably expressed in GL26-Luc cells. Luciferase siRNA or siRNA scramble (5 μg) carried by the FA-pGNVs was intranasally administrated to 15-day GL-26-luc tumor-bearing mice. Imaging data showed a statistically significant decrease in brain-associated photons in FA-pGNVs/siRNA-Luc-treated mice when compared to FA-pGNV/siRNA scramble-treated mice (**Figure 4a**) at 48 hours.

Our published data suggest that one of the miR17-targeted genes is MHC-1.[17] miR17-mediated downregulation of MHC1 expressed on the tumor cells led to activation of NK cells and inhibited tumor growth.[17] Therefore, we tested whether miR17 carried by FA-pGNVs can be delivered to GL-26 brain tumor and achieve a therapeutic effect. qPCR indicated that FA-pGNVs are more efficient in delivering miR17 to GL-26 cells than pGNVs, and the FA-pGNVs are stable 48 hours after transfection (**Supplementary Figure S5**). FACS analysis further indicated that miR17 inhibits MHCI expression on GL-26 cells (**Supplementary Figure S6**). Next, we conducted *in vivo* delivery experiments of miR17 with FA-pGNVs targeting of mouse GL-26 brain tumor to determine the therapeutic effect of miR17. We treated groups of mice bearing intracerebral tumors with FA-pGNV/miR17, FA-pGNV/miRNA scramble, or PBS as a control. Mice were treated every 3 days for 21 days beginning on day 5 after the tumor cells were implanted. The amount of miR17 administered was based on the lack of any evidence of toxicity or behavioral abnormalities in the mice. Twenty-one days after tumor cells were injected imaging data showed a statistically significant decrease in brain-associated photons in FA-pGNV/miR17-treated mice when compared to controls (**Figure 4b**). Survival times of PBS control and FA-pGNV/scramble miRNA animals ranged from 20 to 33 days. In contrast, FA-pGNV/miR17 treatment significantly prolonged

to C57BL/6j mice. At different time points post intranasal administration, the brain was cut sagittally, and the ventral sides of cut brain were placed against the scanner for imaging using the Odyssey laser-scanning imager. Enlarged images are shown at the bottom. (**e**) DIR-labeled GNVs or pGNV/RNA was administered intranasally to C57BL/6j mice. At 12 hours post intranasal administration, the brain was cut sagittally, and the ventral sides of cut brain were placed against the scanner for imaging using the Odyssey laser-scanning imager. (**d**,**e**) Representative sagittal images from the center of the brain ($n = 5$). (**f**) Intranasal administration of pGNVs does not induce brain macrophages. pGNV/RNA or PEI/RNA were administered intranasally to C57BL/6j mice. Mice were sacrificed 12 or 24 hours after intranasal administration of pGNV/RNA or PEI/RNA. C57BL/6j mice were i.p. injected with bacterial lipopolysaccharide (2.5 mg/kg) or PBS as a control and sacrificed at 12 and 24 hours postinjection as a control. Brain tissue sections were fixed as described in the Materials and Methods section. Frozen sections (10 μm) of the anterior part of the brain were stained with the antimicroglial cell marker Iba-1 (green color) or macrophages (red). Slides were examined and photographed using microscope with an attached camera (Olympus America, Center Valley, PA). Each photograph is representative of three different independent experiments ($n = 5$). Original magnification: ×40.

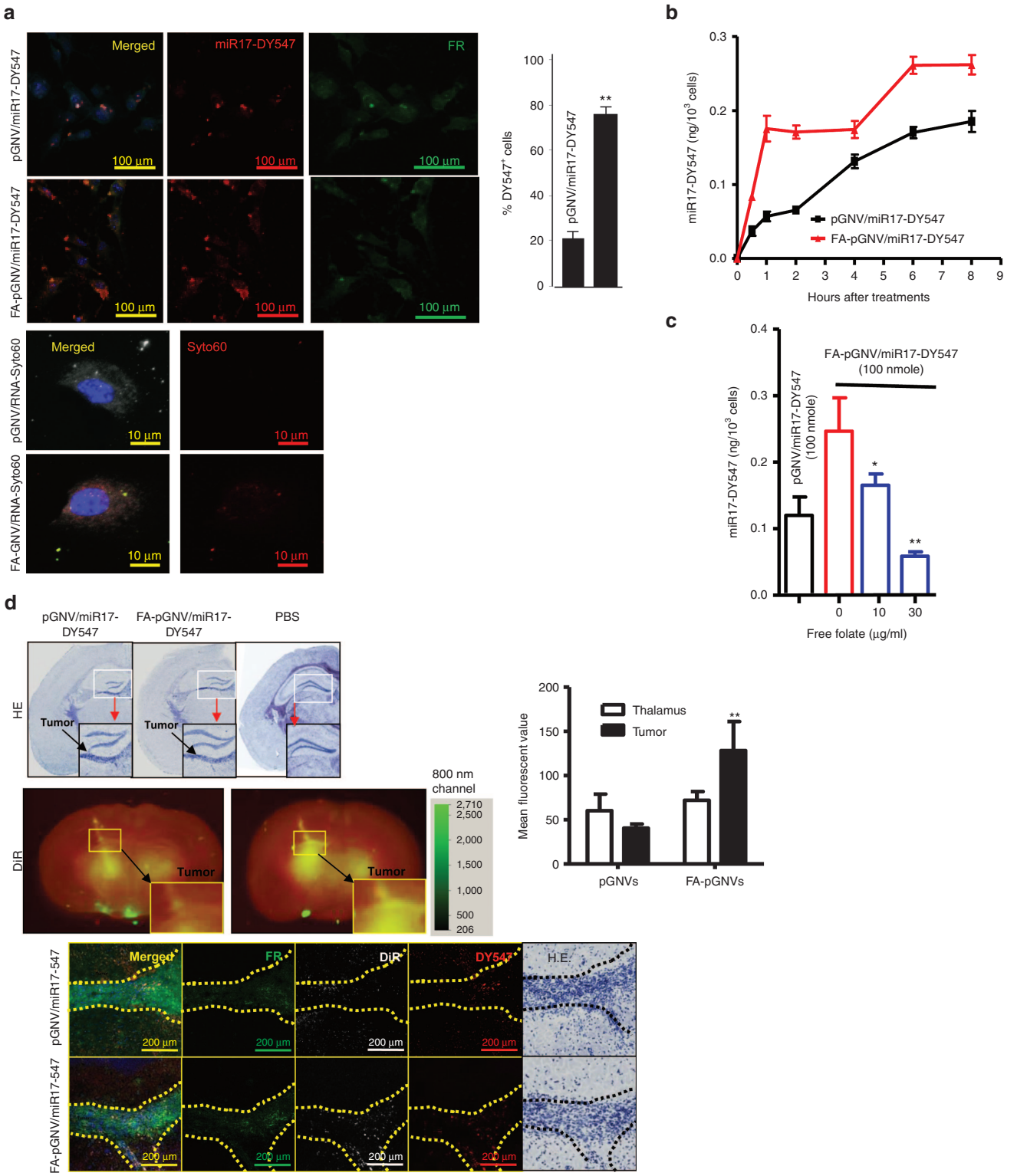

Figure 3 Folate receptor-mediated uptake of FA-pGNVs. GL-26-luc cells were cultured in the presence of Dylight547-labeled miR17 or Syto60-labeled RNA carried by FA-pGNVs (FA-pGNV/miR17-Dy547, FA-pGNV/RNA-Syto60) or by pGNVs (pGNV/miR17-DY547, pGNV/RNA-Syto60). (**a**) Representative images of cells ($n = 3$) were taken at 2 hours after addition of FA-pGNVs/miR17-Dy547, pGNVs/miR17-DY547, FA-pGNV/RNA-Syto60, or pGNV/RNA-Syto60 using a confocal microscope at a magnification of ×200 (top panel) or ×600 (bottom panel) and quantified by counting the number of DY547$^+$ cells in five individual fields in each well. % of DY547$^+$ cells was calculated based on the number of DY547$^+$ cells/numbers of FR$^+$ cells × 100. The results are presented as the mean ± SEM. $^{**}P < 0.01$. (**b**) At different time points, post incubation at 37 °C, transfection efficiency of FA-pGNV/miR17-Dy547 or pGNV/miR17-DY547 was analyzed by measuring fluorescent density using a microplate reader at Ex/Em = 530 /590 nm. (**c**) Before adding to GL-26-luc cultures, FA-pGNV/miR17-Dy547 (100 nmol) was premixed with different concentrations of FA, and then, GL-26-luc cells were cultured in the presence of FA premixed with FA-pGNV/miR17-Dy547 for 2 hours. The effects of folate on the transfection efficiency of FA-pGNV/miR17-Dy547

the survival of mice to an average of 47.5 days ($P < 0.0012$; **Figure 4c**). Although none of the FA-pGNV/miR17-treated animals exhibited evidence of toxicity or behavioral abnormalities during the treatment period, most of the FA-pGNV/miR17-treated surviving mice (8/12) were not tumor free on day 70, on which all of mice were killed for evaluation of brain tumors by hematoxylin and eosin staining. To further investigate if the reduction of tumor cells in the brain is associated with induction of NK cells in the FA-pGNVs/miR17 targeted tumor, the numbers of luciferase expressed GL-26 tumor cells (**Figure 4d**) and of NK cells in the GL-26 tumor (**Figure 4e**) were determined. The results suggest that FA-pGNV/miR17 treatment led to increased numbers of $DX5^+$NK cells in the GL-26 tumor (**Figure 4e**). The induction of $DX5^+$NK cells was also correlated with a decrease in the expression of $MHCI^+$luciferase$^+$ GL-26 tumor cells (**Figure 4e**). Collectively, these data support the idea that FA-pGNV/miR17 is selectively taken up by GL-26 cells and subsequently inhibits the expression of MHCI expressed on the GL-26 tumor cells, which triggers activation of NK cells to kill tumor cells.

DISCUSSION

Although the efficacy of using mammalian cell-derived exosomes as a delivery vehicle for intranasal delivery of therapeutic agents has been demonstrated in mouse models,[4] biosafety considerations and large scale production of mammalian cell-derived exosomes has presented obstacles to their clinical use. The present study examined a novel approach for GNV-mediated intranasal delivery of RNA in general and therapeutic miR17 specifically to the brain tumor cells. Our results clearly indicate that RNA, including miR17, is effectively delivered to the brain by pGNVs without observable side effects. Furthermore, our study advances an approach for targeted delivery of therapeutic miR17. In these studies we used folate acid coated pGNVs (FA-pGNVs) as proof of concept, to demonstrate enhanced targeting to GL-26 glioma tumor cells which express increased amounts of the FR; which promoted much more substantial therapeutic benefits without inducing adverse side-effects. Like other liposomes, the folate ligand could be incorporated into the liposomal bilayer during pGNV preparation by mixing a lipophilic folate ligand with other GNV lipid components. The lipophilic anchor for the folate ligand can be either GNV phospholipid or cholersterol.[18–23] The FA-pGNVs also avoids several of the problems such as the lack of tissue targeting specificity, toxicity, and difficulty in scalability and production, the need for lifelong monitoring for potential tumorigenesis and other adverse clinical outcomes that have arisen with conventional therapy vectors including PEI and DOTAP. Because FA-pGNVs do not cause these concerns they have great potential as targeted delivery vehicles, in particular, because production of GNVs is easily scaled up, and the GNVs can be coated with a variety of targeting moieties. Since chemically synthesized nanovectors are known to induce toxicity,[24–27] which is a major obstacle for clinical use, the approach combining PEI and GNVs as we demonstrated in this study could apply to nanotechnology in general to overcome the potential toxicity for clinical application.

Our data presented in this study show that miR17-mediated induction of NK cells through downregulation of MHCI expressed on the GL-26 tumor cells is one of the mechanisms underlying the therapeutic effects; other mechanisms cannot be excluded for contributing to the antitumor growth as miR17 is a pleiotropic miRNA like other miRNAs that can target multiple pathways. From a therapeutic standpoint, an appealing property of miRNAs as therapeutic agents is their capacity to target multiple genes, making them extremely efficient in regulating distinct biological processes in the context of a network. Genes involving such a network are dysregulated during the development of cancer. Therefore, developing therapeutic strategies to restore homeostasis by delivery of miRNA would be more efficient than targeting individual genes or proteins. In addition, GL-26 cells may be not the only cells targeted by FA-pGNVs. The biological effects of other cells, particularly FA-positive infiltrating immune cells, including myeloid cells on the inhibition of brain tumor progression may also be involved and needs to be further studied.

For more efficient therapeutic outcomes, enhanced selectivity or targeting of nanovector-based delivery vehicles is required to ensure targeting of tumor cells and not healthy normal cells. The enhanced permeability and retention effect in combination with modification of the vector by coating with a targeting moiety have been extensively studied for improving targeting efficiency. However, it is unlikely that 100% of the tumor cells can be targeted. In addition, most of delivery vectors are made of foreign material which is immunogenic and cannot be given repeatedly. In contrast, nonimmunogenic GNVs can be used to carry therapeutic agents including antitumor and/or to stimulation of immune response, simultaneously. This will lead not only to a reduction in tumor size but also to the possible elimination of residual tumor cells that can be chemoresistant.

In this study, we found rapid movement of GNVs into the brain within 1.5 hour of intranasal administration. This finding is consistent with the results generated from mammalian cell EL4-derived exosomes.[4] Collectively, fast and selective homing to the brain of FA-GNVs warrants further exploration for their ability to carry of other types of biological cargo including drugs, therapeutic antibodies, and oncolytic viruses which selectively replicate in tumor cells.

Although our findings demonstrate the potential for using GNVs as a novel, noninvasive delivery vehicle to target therapeutic agents to the brain, more fundamental studies are required, such as the mechanism underlying the GNV-mediated high intranasal

were analyzed by measuring fluorescent density using a microplate reader at Ex/Em = 530/590 nm. Data in **a–c** are the mean ± SEM of two experiments ($n = 5$). (**d**) FA-pGNV/miR17-Dy547 more efficiently targeted brain tumor. 2×10^4 GL26-luc cells per mouse were injected intracranially in 6-week-old wild-type B6 mice. Five-day tumor-bearing mice were then treated intranasally with FA-pGNV/miR17-Dy547 in PBS or pGNV/miR17-Dy547. FA-pGNV/miR17-Dy547 in PBS or pGNV/miR17-Dy547 (red representing miR17 labeled with Dylight 547, 20 μg of miR17 carried by pGNVs) was administered intranasally into C57BL/6j mice. Results of hematoxylin and eosin (HE) staining showing tumor tissue as indicated by arrows (top panel). DIR dye-labeled FA-pGNV/miR17-Dy547 or pGNV/miR17-Dy547 (second panel from the top, the results represent the mean ± SEM of three independent experiments, bar graph). HE-stained brain sections of GL-26-luc tumor-bearing mice (the first column from right) or miR17-Dy547 (red) or anti-folate receptor (FR) antibody stained (green) brain tumor sections and adjacent area of mice treated with the agents listed (third and fourth panel from the top). Original magnification: ×20. Data represent at least three experiments with five mice/group.

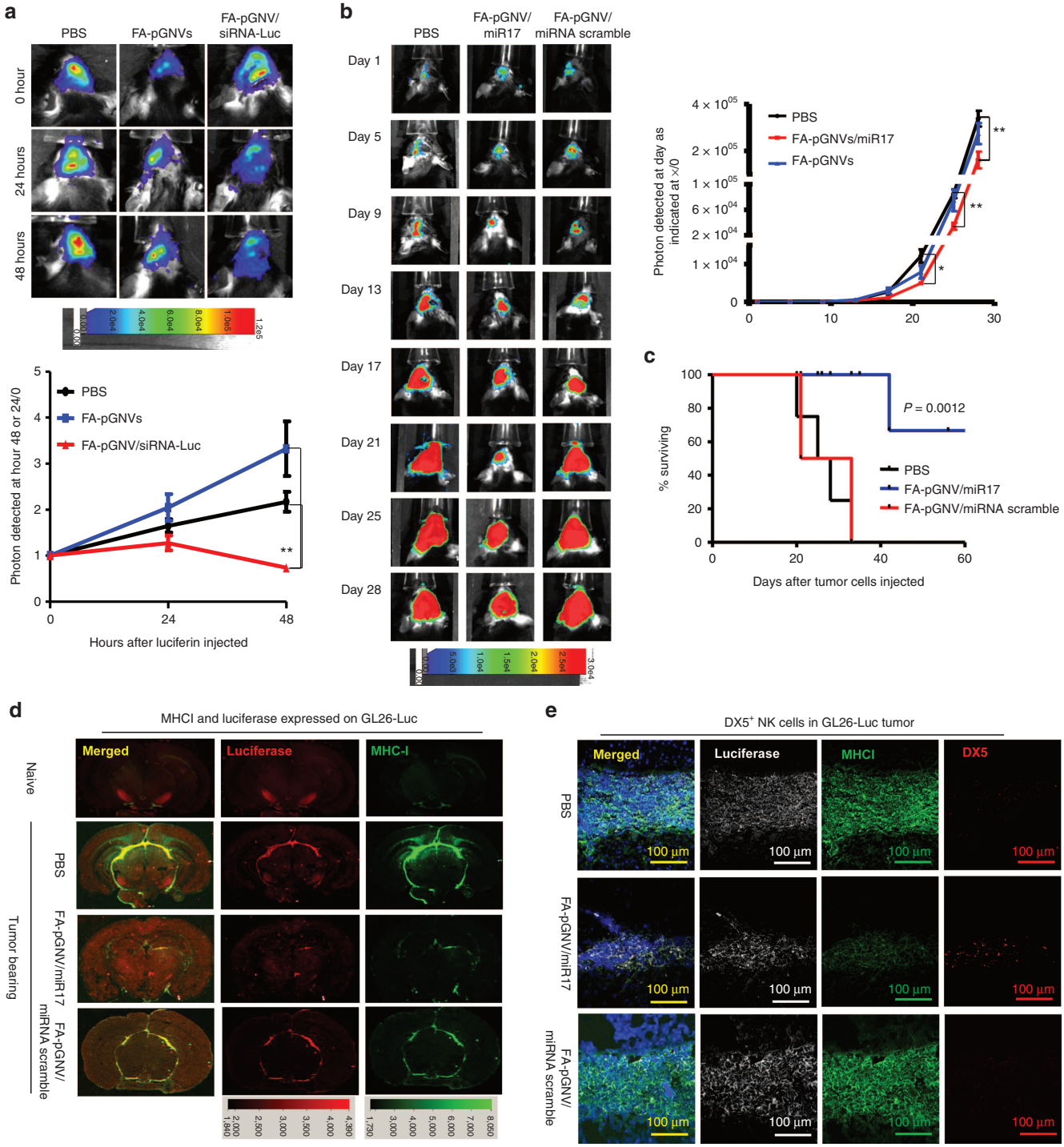

Figure 4 FA-pGNV/miR17-Dy547 treatment prevents the growth of *in vivo* injected brain tumor cells. 2×10^4 GL26-luc cells per mouse were injected intracranially in 6-week-old wild-type B6 mice. Fifteen-day tumor-bearing mice were then treated intranasally on a daily basis with FA-pGNVs/siRNA-luc or FA-pGNVs/siRNA scramble control. The mice were imaged on the hours as indicated in **a**. (**a**) A representative photograph of brain tumor signals of a mouse from each group ($n = 5$) is shown (top panel). *In vitro* time course of bioluminescent signal generated by GL26-Luc cells is shown (bottom panel). The results are based on two independent experiments with data pooled for mice in each experiment ($n = 5$) and are presented as the mean ± SEM. $^{**}P < 0.01$. (**b**) Mice were intracranially injected with GL26-luc and treated every 3 days for 21 days beginning on day 5 after tumor cells were implanted. The mice were imaged on the days as indicated in the labeling of **b**. (**b**) A representative photograph of brain tumor signals of a mouse from each group ($n = 5$) is shown (left). *In vitro* time course of bioluminescent signal generated by GL26-Luc cells is shown (right panel). The results are based on two independent experiments with data pooled for mice in each experiment ($n = 5$) and are presented as the mean ± SEM; $^{*}P < 0.05$, $^{**}P < 0.01$. (**c**) Percent of FA-pGNVs/miR17, FA-pGNVs/scramble miRNA, or PBS mice surviving was calculated. One representative experiment of four independent experiments is shown ($n = 5$ females per group). (**d**) Results of anti-luciferase and MHCI staining or (**e**) antiluciferase/MHCI/DX5 staining of brain tumor sections and adjacent area of mice treated with the agents listed. Original magnification: ×20. Data represent at least three experiments with five mice per group.

transporting efficiency versus poor transporting efficiency of DOTAP. Additional research is also necessary to study the mechanism of GNV translocation from the nasal cavity to the brain and identify the route by which GNVs travel to the olfactory bulb and ultimately throughout the nervous system. In addition, we noticed that the signal from DIR-labeled pGNVs is weaker than that from Syto60-labeled pGNVs (**Figure 2d**). This could be due to having multiple copies of Syto60-labeled RNA that are complexed with one copy of GNV. Therefore, the signal generated from Syto60-labeled RNA is the more intense signal. It is also possible that Syto60 is less affected (more stable) during trafficking from the nose to the brain than DiR dye, which would explain the higher signal intensity.

MATERIALS AND METHODS

Reagents. DOTAP/DOPE mixture (790310C) was purchased from Avanti Polar Lipids. The Dual-Luciferase Report Assay System was purchased from Promega. Luciferase GL3 Duplex was purchased (Dharmacon). miR-17 mimics (sequence: CAAAGUGCUUACAGUGCAGGUAG, catalog number: 4464066, Life Technologies) and Dylight547-labeled miR17 (sequence: UGGAAGACUAGUGAUUUUGUUGU-DY547) was synthesized by Life Technologies. Near-infrared fluorescein dye DiIC18(7) (1,1′-dioctadecyl-3,3,3′,3′-tetramethylindotricarbocyanine iodide) (DiR) and SYTO 60 Red Fluorescent dye (Syto60) was purchased from Life Technologies. Polyethylenimine, branched (average MW~25000, catalog number: 408727), FA, glutaraldehyde, cacodylate buffer, sucrose, and paraformaldehyde were purchased from Sigma.

The following antibodies were used: rabbit anti-Iba1 antibody that specifically recognizes microglial cells and macrophages (Wako Chemicals, Richmond, VA), anti-FR(N-20) (Santa Cruz Biotechnology), anti-luciferase (Santa Cruz Biotechnology), anti-F4/80 (BM8, eBioscience), antimouse MHC Class I (eBioscience), antimouse CD49b (DX5) (eBioscience), IRDye 800CW goat antimouse IgG (H + L) (LI-COR Biosciences, Lincoln, Nebraska). The following secondary antibodies were purchased from Life Technologies: Alexa fluor 594-conjugated goat antirat IgG (H+L) (A11007), Alexa fluor 488-conjugated rabbit antimouse IgG (H+L) (A11059), Alexa fluor 488-conjugated chicken anti-goat IgG (H+L) (A21467), Alexa fluor 680-conjugated goat antirabbit IgG (H+L) (A21109), and Alexa fluor 488-conjugated goat antirabbit IgG (H+L) (A11008).

Cell line. The mouse (H-2b) glioblastoma cell line GL-26 stably expressing the luciferase gene (GL26-Luc) was provided by Dr Behnam Badie (Beckman Research Institute of the City of Hope, Los Angeles, CA) and maintained in RPMI-1640 media supplemented with 10% heat-inactivated fetal bovine serum in a humidified CO_2 incubator at 37 °C.

Animals. C57BL/6j mice (H-2b) were purchased from the Jackson Laboratory (Bar Harbor, ME). Animals were housed in the animal facility at the University of Louisville per an Institutional Care and Use Committee–approved protocol.

Preparation of grapefruit-derived nanovectors GNVs, pGNVs, and FA-pGNVs. All GNVs used in this study were prepared according to a previously described protocol.[6] pGNVs were made of PEI/RNA and GNV complex. PEI/RNA complex was formed by adding PEI in PBS to RNA extracted from EL4 cells, synthetized miR17, or Dylight 547-labeled miR17 (miR17-Dy547) or siRNA-luc or scramble siRNA (PEI/RNA = 10:1, in weight), and the mixtures were then incubated at 25 °C for 30 minutes for formation of PEI/RNA complex. The PEI/RNA complex was added to the film of lipids extracted from grapefruit nanoparticles using a described method.[6] Samples were sonicated in a bath-sonicator (FS60 bath sonicator; Fisher Scitific, Pittsburg, PA) for 15 minutes, and sonication repeated three times and followed by ultracentrifuge at 100,000*g* for 90 minutes at 4 °C to wash unbound RNA or PEI/RNA from the PEI/RNA/GNV complexes. The efficiency of RNA associated with pGNVs was demonstrated by measuring the amount of RNase predigested miR17-Dy547 encapsulated in pGNVs (pGNV/miR17-Dy547) using a fluorescence microplate reader (EX/Em = 530/590 nm). The amount of miR17 carried by the pGNVs was calibrated based on a comparison to a standard curve generated from synthesized miR17-Dy547 of known concentrations and expressed as ng of Dy547-miR17/1mM of GNVs. The efficiency of miR17 carried by pGNVs was expressed as % = amounts of miR17-Dy547 carried by pGNVs/total amounts of miR17-Dy547 initially added to PEI or GNVs × 100. Before being used in experiments, the pGNVs were homogenized by passing them through a high pressure homogenizer (Avestin, Ottawa, Canada) using a protocol provided in the homogenizer instruction manual. For production of FA-pGNVs, total lipids was extracted from sucrose-purified grapefruit nanoparticles by the Bligh and Dyer method[28] and quantified using the phospholipid assay of Rouser.[29] FA (12.5 µg in dimethyl sulfoxide) was added to the lipid (1 mmol/l phospholipid in chloroform) extracted from grapefruit nanoparticles, and a film was formed by being dried under nitrogen gas before adding the PEI-RNA complex to make FA-pGNVs using an identical protocol as described for making pGNVs. The density of sucrose-banded GNV, GNV/RNA, and pGNV/RNA was determined by measuring the refractive index of a 10-µl aliquot with an Abbe refractometer (Leica Mark II plus) at a constant temperature of 20 °C. The PEI associated with PEI/RNA and pGNVs was quantitatively analyzed with a method as described.[30]

Intranasal delivery of GNVs, pGNVs, and FA-pGNVs in mice. For intranasal administration of GNVs, pGNVs, and FA-pGNVs, C57BL/6j mice were anesthetized by i.p. injection of a ketamine/xylazine mixture (40 mg/5 mg/kg body weight) and each mouse placed in a supine position in an anesthesia chamber. PBS (2 µl) containing GNVs, pGNVs, or FA-pGNVs (20 nmol/2 µl) was administered intranasally as drops with a small pipette every 2 minutes into alternating sides of the nasal cavity for a total of 20 minutes. A total volume of 20 µl was delivered into the nasal cavity.

Evaluation of brain inflammation. Mice were administered intranasally with pGNVs or PEI-RNA complex (3.0 µg RNA/mouse) using the method described above. Bacterial LPS (2.5 mg/kg; Sigma-Aldrich) was injected intraperitoneally into C57BL/6j mice as a control for induction of brain inflammation. After intranasal administration, mice were transcardially perfused with PBS followed by a 2% paraformaldehyde solution at pH 7.4. Brain tissue was postfixed for 2 h in 2% paraformaldehyde and then cryopreserved in phosphate-buffered 30% sucrose. Brains were embedded in optimal cutting temperature compound (Tissue-Tek; Sakura, Torrance, CA) and kept at −20 °C overnight. Brain tissue sections were cut with a cryostat (10 µm thick), and the tissue sections stored at −20 °C. Immunofluorescent staining of microglial cells with rabbit anti-Iba1 antibody or F4/80 antibody was carried out according to previously described procedures. Tissues evaluated for the presence of Iba1 or F4/80 positive staining were assessed using a Nikon A1R confocal microscope equipped with a digital image analysis system (Pixera, San Diego, CA).

Ex vivo *imaging.* To monitor the trafficking of GNVs administered intranasally, GNVs were first labeled using a near-infrared lipophilic carbocyanine dye-dioctadecyl-tetramethylindotricarbocyanine iodide (DIR; Invitrogen, Carlsbad, CA) using a previously described method.[6,31–34] To localize GNVs in brain tissue, the DIR-labeled GNVs (10 µg/10 µl in PBS) were administered intranasally to C57BL/6j mice as described above. The brains of treated mice were imaged over a 24-hour period using a prototype LI-COR imager (LI-COR Biosciences). For controls, mice (five per group) received either DOTAP liposomes or nonlabeled GNVs in PBS or free DIR dye at the same concentration for DIR dye-labeled GNVs.

Brain tumor-bearing mice model. GL26-Luc cells were intracranially injected per mouse using a method described previously.[4] In brief, 2 µl of PBS containing 5×10^4 tumor cells were injected unilaterally at the coronal

suture, 1 mm lateral to the midline, and 3 mm deep into the frontal lobes, using a Hamilton syringe (Fisher Scientific). Tumor-bearing mice were treated every 3 days for 21 days beginning on day 5 after the tumor cells were implanted at a dose of 20 μg of miR17 or miRNA scramble carried by FA-pGNVs or FA-pGNVs in PBS as a control. All mice were monitored every day and euthanized when they exhibited neurological symptoms indicative of impending death. Monitoring the growth of injected tumor cells was accomplished by quantifying luciferase activity over a 28-day period at 5 days after tumor cell injection using a previously described method.[4] For evaluating the tumor targeted delivery efficiency of FA-pGNVs, siRNA luciferase was carried by FA-pGNVs (FA-pGNV/siRNA luciferase) and 15-day tumor-bearing mice were intranasally administrated FA-pGNV/siRNA luciferase or FA-pGNV/scramble siRNA as a control and luciferase activity of brain tumor-bearing mice was analyzed. Regions of interest were analyzed for luciferase signals using Living Image 2.50 software (Xenogen) and were reported in units of relative photon counts per second. The total photon count per minute (photons/minute) was calculated (five animals) using Living Image software. The effects of treatment versus nontreatment on brain tumor-bearing mice was determined by dividing the number of photons collected for treated mice at different imaging time points by the number of photons collected at zero imaging time. Results were represented as pseudocolor images indicating light intensity. The effects of treatment versus nontreatment on brain tumor-bearing mice on the induction of DX5 NK cells in the GL-26-luc tumor was also evaluated by immune staining of post-fixed brain tissue with anti- DX5, luciferase, and MHCI antibodies according to previously described procedures.[4,17]

Size and surface charge of GNV, pGNVs, and FA-pGNVs were determined by Zetasizer Nano S90.

Electron microscopy analysis. GNVs were fixed with 2% glutaraldehyde in 0.1 mol/l cacodylate buffer (pH 7.4) for 4 hours at 4 °C. After an extensive wash in the same buffer, samples were removed, postfixed for 1 hour at 22 °C with 1% osmium tetroxide in 0.1 mol/l cacodylate buffer (pH 7.4) and coated with gold-palladium, and observed with a Zeiss Supra 35 VP at an accelerating voltage of 10 kV.

Cellular FA-pGNVs uptake experiments. The folate-mediated targeting efficiency of FA-pGNVs was determined by *in vitro* incubation of GL-26-luc cells with miR17-Dy547-loaded or Syto60-labeled RNA-loaded folate-pGNVs. Briefly, after removing the culture medium, cells were washed once with PBS and RPMI 1640 (200 μl) then added to each well. FA-pGNV/miR17-Dy547, pGNV/miR17-Dy547, FA-pGNV/Syto60-RNA, or pGNV/Syto60-RNA (0.5 nmol/μl) was added to each well. Cells were then incubated for variable time points at 37 °C in a 5% CO_2 incubator. Following incubation, cells were placed on ice, washed three times with 100 μl of ice-cold PBS to remove extracellular FA-pGNVs/miR17-Dy547, pGNVs/miR17-Dy547, FA-pGNVs/Syto60-RNA, or pGNVs/Syto60-RNA. The fluorescence intensity of the cells was measured using a fluorescence spectrometer (Synergy HT, BioTek) at an excitation/emission of 530/590 nm or Dylight547-labeled miR17$^+$ cells (red) or Syto60-labeled RNA were assessed with Nikon A1R confocal microscope equipped with a digital image analysis system (Pixera, San Diego, CA).

The amount of miR17 in the transfected GL-26 cells was quantitatively analyzed with qPCR using a described method.[17] The specificity of the folate-targeted FA-pGNV/miR17-Dy547 for GL-26-luc cells expressing the FR was determined by performing cellular competitive binding experiments. In these experiments, FA-pGNVs/miR17-Dy547 (0.5 nmol/μl) was premixed with variable amount of free folate, and then, mixed samples were added to a 12 hours culture of GL-26-luc cells. miR17-Dy547 concentrations in cells were determined by measuring Dylight547 from microplate reader at Ex/Em = 530/590 nm.

Flow cytometry. GL-26-luc cell lines were digested and centrifuged at 800*g*, and cell pellets were resuspended in FACS buffer (PBS, 1% BSA, 0.1% EDTA). Cells were pretreated on ice with the FcγR-blocking mAb (eBioscience) for 10 minutes. This step was followed by treating with anti-mouse MHC class I (eBioscience) for 30 minutes on ice. All data were analyzed using FlowJo FACS software.

Statistical analysis. Survival data were analyzed by log rank test. Student's *t*-test was used for comparison of two samples with unequal variances. One-way ANOVA with Holm's *post hoc* test was used for comparing means of three or more variables.

SUPPLEMENTARY MATERIAL

Figure S1. Characterization of GNV-based nanovector hybrid with polyethylenimine (PEI).
Figure S2. pGNV/RNA has a higher sucrose density than GNVs.
Figure S3. The same amount of PEI detected in the PEI/RNA and pGNV/RNA.
Figure S4. GL-26 tumor cells express FRs.
Figure S5. FA-pGNVs are more efficient in delivering miR17 to GL26 cells than pGNVs.
Figure S6. Reduction of MHC class I on GL26-luc tumor cells by miR-17 encapsulated in FA-pGNVs.

ACKNOWLEDGMENTS

This work was supported by grants from the National Institutes of Health (NIH) (UH2TR000875) and the Louisville Veterans Administration Medical Center (VAMC) Merit Review Grants (H.-G.Z.). The authors thank Behnam Badie (Beckman Research Institute of the City of Hope, Los Angeles, CA) for providing GL26-Luc and Jerald Ainsworth for editorial assistance.

REFERENCES

1. Ong, WY, Shalini, SM and Costantino, L (2014). Nose-to-brain drug delivery by nanoparticles in the treatment of neurological disorders. *Curr Med Chem* **21**: 4247–4256.
2. Kozlovskaya, L, Abou-Kaoud, M and Stepensky, D (2014). Quantitative analysis of drug delivery to the brain via nasal route. *J Control Release* **189**: 133–140.
3. Larsen, JM, Martin, DR and Byrne, ME (2014). Recent advances in delivery through the blood-brain barrier. *Curr Top Med Chem* **14**: 1148–1160.
4. Zhuang, X, Xiang, X, Grizzle, W, Sun, D, Zhang, S, Axtell, RC *et al.* (2011). Treatment of brain inflammatory diseases by delivering exosome encapsulated anti-inflammatory drugs from the nasal region to the brain. *Mol Ther* **19**: 1769–1779.
5. Wang, Q, Ren, Y, Mu, J, Egilmez, NK, Zhuang, X, Deng, Z, *et al.* (2015). Grapefruit-derived nanovectors use an activated leukocyte trafficking pathway to deliver therapeutic agents to inflammatory tumor sites. *Cancer Res* **75**: 2520–2529.
6. Wang, Q, Zhuang, X, Mu, J, Deng, ZB, Jiang, H, Zhang, L *et al.* (2013). Delivery of therapeutic agents by nanoparticles made of grapefruit-derived lipids. *Nat Commun* **4**: 1867.
7. Islam, MA, Park, TE, Singh, B, Maharjan, S, Firdous, J, Cho, MH *et al.* (2014). Major degradable polycations as carriers for DNA and siRNA. *J Control Release* **193**: 74–89.
8. Buzea, C, Pacheco, II and Robbie, K (2007). Nanomaterials and nanoparticles: sources and toxicity. *Biointerphases* **2**: MR17–MR71.
9. Patnaik, S and Gupta, KC (2013). Novel polyethylenimine-derived nanoparticles for *in vivo* gene delivery. *Expert Opin Drug Deliv* **10**: 215–228.
10. Chaudhury, A and Das, S (2015). Folate receptor targeted liposomes encapsulating anti-cancer drugs. *Curr Pharm Biotechnol* **16**: 333–343.
11. Marchetti, C, Palaia, I, Giorgini, M, De Medici, C, Iadarola, R, Vertechy, L *et al.* (2014). Targeted drug delivery via folate receptors in recurrent ovarian cancer: a review. *Onco Targets Ther* **7**: 1223–1236.
12. Serpe, L, Gallicchio, M, Canaparo, R and Dosio, F (2014). Targeted treatment of folate receptor-positive platinum-resistant ovarian cancer and companion diagnostics, with specific focus on vintafolide and etarfolatide. *Pharmgenomics Pers Med* **7**: 31–42.
13. Muller, C (2012). Folate based radiopharmaceuticals for imaging and therapy of cancer and inflammation. *Curr Pharm Des* **18**: 1058–1083.
14. Franzen, S (2011). A comparison of peptide and folate receptor targeting of cancer cells: from single agent to nanoparticle. *Expert Opin Drug Deliv* **8**: 281–298.
15. Dhawan, D, Ramos-Vara, JA, Naughton, JF, Cheng, L, Low, PS, Rothenbuhler, R *et al.* (2013). Targeting folate receptors to treat invasive urinary bladder cancer. *Cancer Res* **73**: 875–884.
16. Leamon, CP, Reddy, JA, Vetzel, M, Dorton, R, Westrick, E, Parker, N *et al.* (2008). Folate targeting enables durable and specific antitumor responses from a therapeutically null tubulysin B analogue. *Cancer Res* **68**: 9839–9844.
17. Jiang, H, Wang, P, Li, X, Wang, Q, Deng, ZB, Zhuang, X *et al.* (2014). Restoration of miR17/20a in solid tumor cells enhances the natural killer cell antitumor activity by targeting Mekk2. *Cancer Immunol Res* **2**: 789–799.
18. Kularatne, SA and Low, PS (2010). Targeting of nanoparticles: folate receptor. *Methods Mol Biol* **624**: 249–265.
19. Zhao, XB, Muthusamy, N, Byrd, JC and Lee, RJ (2007). Cholesterol as a bilayer anchor for PEGylation and targeting ligand in folate-receptor-targeted liposomes. *J Pharm Sci* **96**: 2424–2435.
20. Dauty, E, Remy, JS, Zuber, G and Behr, JP (2002). Intracellular delivery of nanometric DNA particles via the folate receptor. *Bioconjug Chem* **13**: 831–839.

21. Wang, H, Zheng, X, Behm, FG and Ratnam, M (2000). Differentiation-independent retinoid induction of folate receptor type beta, a potential tumor target in myeloid leukemia. *Blood* **96**: 3529–3536.
22. Reddy, JA, Dean, D, Kennedy, MD and Low, PS (1999). Optimization of folate-conjugated liposomal vectors for folate receptor-mediated gene therapy. *J Pharm Sci* **88**: 1112–1118.
23. Mayor, S, Sabharanjak, S and Maxfield, FR (1998). Cholesterol-dependent retention of GPI-anchored proteins in endosomes. *EMBO J* **17**: 4626–4638.
24. Ding, L, Liu, Z, Aggrey, MO, Li, C, Chen, J and Tong, L (2015). Nanotoxicity: the toxicity research progress of metal and metal-containing nanoparticles. *Mini Rev Med Chem* **15**: 529–542.
25. Czajka, M, Sawicki, K, Sikorska, K, Popek, S, Kruszewski, M and Kapka-Skrzypczak, L (2015). Toxicity of titanium dioxide nanoparticles in central nervous system. *Toxicol In Vitro* **29**: 1042–1052.
26. Zoroddu, MA, Medici, S, Ledda, A, Nurchi, VM, Lachowicz, JI and Peana, M (2014). Toxicity of nanoparticles. *Curr Med Chem* **21**: 3837–3853.
27. Nafisi, S, Schäfer-Korting, M and Maibach, HI (2015). Perspectives on percutaneous penetration: Silica nanoparticles. *Nanotoxicology* **9**: 643–657.
28. Bligh, EG and Dyer, WJ (1959). A rapid method of total lipid extraction and purification. *Can J Biochem Physiol* **37**: 911–917.
29. Rouser, G, Siakotos, AN and Fleischer, S (1966). Quantitative analysis of phospholipids by thin-layer chromatography and phosphorus analysis of spots. *Lipids* **1**: 85–86.
30. Ungaro, F, De Rosa, G, Miro, A and Quaglia, F (2003). Spectrophotometric determination of polyethylenimine in the presence of an oligonucleotide for the characterization of controlled release formulations. *J Pharm Biomed Anal* **31**: 143–149.
31. Youniss, FM, Sundaresan, G, Graham, LJ, Wang, L, Berry, CR, Dewkar, GK *et al.* (2014). Near-infrared imaging of adoptive immune cell therapy in breast cancer model using cell membrane labeling. *PLoS One* **9**: e109162.
32. Ezzat, T, Dhar, DK, Malago, M and Olde Damink, SW (2012). Dynamic tracking of stem cells in an acute liver failure model. *World J Gastroenterol* **18**: 507–516.
33. Cho, H, Indig, GL, Weichert, J, Shin, HC and Kwon, GS (2012). *In vivo* cancer imaging by poly(ethylene glycol)-b-poly(ε-caprolactone) micelles containing a near-infrared probe. *Nanomedicine* **8**: 228–236.
34. Shan, L (2004). *Near-Infrared Fluorescence 1,1-Dioctadecyl-3,3,3,3-Tetramethylindotricarbocyanine Iodide (DiR)-Labeled Macrophages for Cell Imaging*. Molecular Imaging and Contrast Agent Database (MICAD): Bethesda, MD.